



OPEN

Investigation into the temporal impacts of drought on vegetation dynamics in China during 2000 to 2022

Yutian Du¹, Subing Lv^{1,2}, Fuqiang Wang^{1,2}✉, Jie Xu¹, Heng Zhao^{1,2}, Lei Tang^{1,2}, Heng Wang¹ & Honglu Zhang¹

Quantifying vegetation's response to drought and understanding its mechanisms is crucial for mitigating the adverse effects of drought disasters. The asymmetric cumulative and lag effects of drought on vegetation growth are widespread, yet the responses of different vegetation types, climate zones, and elevations in China remain unclear. This study used the Standardized Precipitation Evapotranspiration Index (SPEI) and Normalized Difference Vegetation Index (NDVI) to analyze vegetation status and drought trends from 2000 to 2022, examining the differentiation and mechanisms of cumulative (CED) and lag effect of drought (LED) under various conditions. The main findings are as follows: (1) 85.1% of the study area is becoming greener, with an overall growth rate of 0.026 per decade. Annual drought levels fluctuate, with increasingly severe conditions in parts of southwestern and northwestern China. (2) CED affects 35.94% of vegetated areas, with 77.44% showing a positive correlation between SPEI and NDVI. Grasslands have the longest CED (5.90 months), while forests have the shortest (4.72 months). Temperate and Arid climate zones show higher CED, at 6.91 months and 6.77 months, respectively. The highest CED is found at elevations of 2000–2500 m (6.34 months), and the lowest at 3000–3500 m (4.28 months). (3) LED affects a larger area (39.22%) with an average duration of 6.42 months, greater than the average CED (5.56 months). Grasslands have the longest LED (7.72 months), while forests (6.78 months) and shrublands (6.48 months) are shorter. The Arid climate zone has the highest LED (8.35 months), and the Tropical zone the lowest (4.82 months). LED shows significant elevation differences, being smallest at low elevations (6.48 months). (4) Climate type and potential evapotranspiration explain 0.269 and 0.259 of CED, respectively. For LED, temperature and potential evapotranspiration are dominant (0.173 and 0.167). The combination of factors significantly enhances the explanatory power of temporal effects. (5) NDVI stability is negatively influenced by CED. This study enhances understanding of the vegetation-drought relationship in China and provides theoretical support for addressing drought risks under climate change.

Keywords NDVI, SPEI, Lag effect, Cumulative effect

Drought is a typical extreme climate event that usually occurs under conditions of insufficient soil moisture supply and high atmospheric water demand¹. It has long caused various adverse impacts on global water resource systems, agricultural production, and natural ecosystems^{2,3}. Vegetation, as a critical component of terrestrial ecosystems, is essential for regulating climate and maintaining the water-carbon balance⁴. Severe drought stress can affect vegetation growth and recovery⁵, and can even lead to secondary ecological disasters such as desertification, soil erosion, and river drying⁶. With the continuing impact of global warming, the frequency and intensity of drought events have significantly increased^{7,8}, adding greater uncertainty to the vegetation-drought relationship⁹. Therefore, understanding the mechanisms of drought's impact on vegetation is crucial for grasping ecosystem vulnerability in the context of climate change and formulating mitigation strategies.

Accurate monitoring of drought is a challenging task in understanding the vegetation-drought relationship. Meteorological drought, agricultural drought, hydrological drought, and socio-economic drought are the four

¹North China University of Water Resources and Electric Power, Zhengzhou 450046, Henan, China. ²Henan Key Laboratory of Water Resources Conservation and Intensive Utilization in the Yellow River Basin, Zhengzhou 450046, Henan, China. ✉email: wangfuqiang@ncwu.edu.cn

types of droughts commonly mentioned in research, with meteorological drought being considered the initial trigger in the drought disaster chain and receiving extensive study^{10–12}. For quantifying meteorological drought, commonly used indices include the Standardized Precipitation Index (SPI)¹³, the Palmer Drought Severity Index (PDSI)¹⁴, and the Standardized Precipitation Evapotranspiration Index (SPEI)¹⁵. SPI has the advantages of multiple time scales and simple calculation^{16,17}, but it only considers precipitation, which limits its application potential in drought and semi-arid regions heavily influenced by temperature (TEM) and evapotranspiration (ET)¹⁸. PDSI includes information on temperature and soil moisture, but its single time scale restricts its flexibility in monitoring the spatio-temporal dynamics of drought¹⁵. In comparison, SPEI uses the difference between precipitation (PRE) and potential evapotranspiration (PET) to assess water deficiency, combining the flexibility of SPI's multiple time scales with PDSI's sensitivity to evapotranspiration^{15,19}, making it more advantageous in drought research. Despite SPEI providing valuable information for drought monitoring, currently available datasets have relatively coarse spatial resolution ($> 0.5^{\circ}$)²⁰, necessitating more refined SPEI data for studying the complex vegetation-drought relationship.

The temporal effects in vegetation-drought interactions are considered significant phenomena, characterized by their asymmetry, including drought lag effects (LED) and drought cumulative effects (CED)^{21–23}. Early studies focused mainly on concurrent impacts of drought, referring to immediate changes in vegetation in response to drought weather²⁴, such as reducing productivity levels and alleviating evapotranspiration through lowering stomatal density, reducing stomatal aperture, or regulating the duration of stomatal opening²⁵. As understanding of drought impacts deepened, research gradually shifted towards long-term effects, particularly LED and CED. LED was first proposed by McDowell, et al.²⁶ in forest ecosystem studies, emphasizing that vegetation recovery after a drought event is not instantaneous, especially in areas with high drought intensity, where recovery may take months or even years. Unlike LED, CED considers the impact of sustained drought conditions on the current state of vegetation, building on LED and representing the cumulative impact of previous periods. The concept of CED was proposed by Vicente-Serrano, et al.¹⁵, highlighting that consecutive drought events can lead to cumulative suppression of vegetation growth, gradually weakening the vegetation's recovery ability, especially over multiple years of drought. CED typically arises from sustained soil moisture deficit between drought events, leading to soil structure degradation and damage to plant root systems, thereby making vegetation recovery more difficult^{21,27}.

The temporal effects of drought on vegetation have been increasingly studied, but most current research focuses on single vegetation types or climatic zones, lacking consideration of complex conditions¹². Researchers have concentrated on the impacts of drought on grasslands; for example, Liu, et al.²⁸ found that 69.98% of grasslands in Central Asia were deeply affected by LED in their NPP study. Wei, et al.²³ found that more than three-quarters (78.55%) of global grasslands were affected by drought CED. While grasslands are one of the most widely distributed terrestrial ecosystems²⁹, global vegetation diversity means different plant species have varying sensitivity to drought^{30,31}, leading to differences in drought temporal effects that cannot be ignored. From the perspective of climatic zones, studies are often conducted in arid and semi-arid regions; for instance, Xu, et al.³² found that the biotic community response in most parts of northern China aligns with drought trends. Zhao, et al.³¹ showed in their study of the Loess Plateau that drought significantly affects 80.81% of grasslands with a CED of 5 to 10 months. Wang, et al.³³ found that 14.3%/12.0% (SPI/SPEI) of vegetation growth on the Qinghai-Tibet Plateau is significantly affected by drought. Under the background of global warming, drought not only occurs more frequently but also affects a broader range, leading to more severe impacts on ecosystems in semi-humid and humid zones lacking drought adaptability. Additionally, the water-thermal conditions vary at different elevations, necessitating investigation into the temporal effects of drought across different elevation gradients²⁸.

China, with its vast territory, rich vegetation types, and complex climatic conditions, is one of the countries most severely affected by drought disasters globally³⁴. However, most previous studies on drought temporal effects have focused on grasslands in northern arid and semi-arid regions, leaving the responses and influencing factors of vegetation to drought temporal effects under different vegetation types, elevation gradients, and climatic conditions across China unclear. NDVI is considered a reliable indicator of vegetation greenness and vitality on regional and continental scales, often used to observe vegetation growth status³⁵. In light of these issues, this study uses NDVI and 5 km resolution SPEI to monitor vegetation growth status and indicate drought, aiming to quantify the differences in temporal effects of drought on vegetation across vegetation types, climates, and elevations, and analyze the driving mechanisms. Specifically, our objectives are: (1) to analyze the trends of drought and vegetation over the past 20 years; (2) to analyze the spatial distribution of drought's cumulative effects and lag effects on vegetation growth; (3) to quantify the differences in temporal effects of drought on vegetation growth status across different climatic zones, vegetation types, and elevation gradients; and (4) to analyze the influencing factors of drought temporal effects, exploring the impact of drought temporal effects on vegetation stability. These results are significant for formulating sustainable ecosystem protection strategies.

Materials and methods

Study area

China spans from approximately latitude $3^{\circ}51'$ to $53^{\circ}34'N$ and longitude $73^{\circ}29'$ to $135^{\circ}04'E$, encompassing a land area of approximately 9.63 million square kilometers. The terrain generally slopes from west to east and is divided into three elevation tiers: mountainous, plateau, and hilly regions, which collectively account for about 67% of the land area, while basins and plains make up approximately 33%. With its vast expanse, China spans a wide range of latitudes, varying distances from the sea, and diverse topographical features and mountain ranges, leading to a variety of climates. According to the Köppen-Geiger climate classification map published by Beck, et al.³⁶, the study area mainly encompasses fifteen subtypes within five categories (Fig. 1a). The vegetation cover in the study area is approximately 71.4%, with a rich diversity of vegetation types. Grasslands and croplands together account for over half of the vegetation cover (56.4%), with grasslands predominantly occur across the

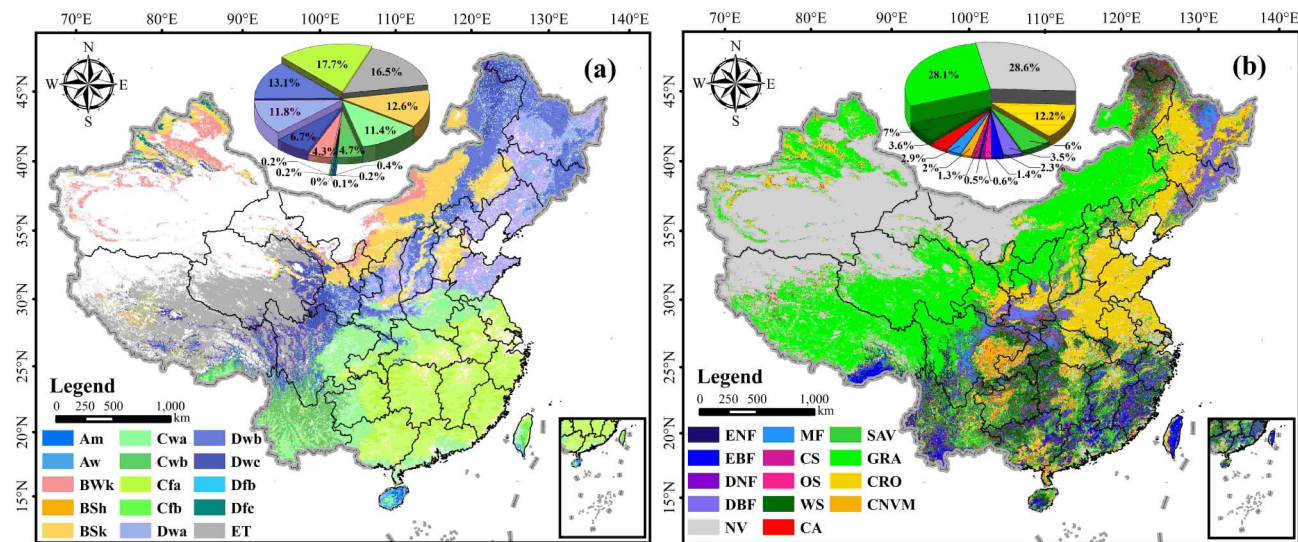


Fig. 1. Köppen-Geiger climate classification (a) and vegetation type map (b) (the maps are based on the standard map produced under the supervision of the Ministry of Natural Resources of the People's Republic of China: Approval number GS (2023) 2763, <http://bzdt.ch.mnr.gov.cn/>, created by ArcMap, version 10.8, <http://www.esri.com/>).

| Data type | Data name | Time series | Spatial resolution | Temporal resolution | Source |
|----------------------|------------------------------|-------------|--------------------|---------------------|---|
| NDVI dataset | MOD13A2 | 2000~2022 | 1 km | 16 days | https://lpdaac.usgs.gov/ |
| Climate dataset | Temperature, | 1901~2022 | 0.00833° | Monthly | http://data.tpdc.ac.cn |
| | Precipitation, | | | | |
| | Potential evapotranspiration | 1990~2022 | | | |
| Vegetation type data | MCD12Q1 | 2000~2022 | 500 m | Yearly | http://lpdaac.usgs.gov/ |
| Climatic zones | Köppen climate data | 1991~2020 | 0.01° | | https://www.globo2.org/koppen/ |
| Elevation | Copernicus DEM | | 90 m | | https://panda.copernicus.eu/ |
| Drought dataset | SPEI | 2000~2022 | 5 km | Monthly | |

Table 1. Details of data sources.

Qinghai-Tibet Plateau, northern Xinjiang, Loess Plateau, and Inner Mongolia, while croplands are primarily situated in the Northeast Plain, North China Plain, and the middle to lower reaches of the Yangtze River (Fig. 1b).

Data sources

The dataset employed in this study comprises NDVI data, meteorological data, vegetation type data, Köppen-Geiger climate classification data, and digital elevation data, with details of each data source provided in Table 1. The global SPEI database SPEIbase provides drought monitoring data at multiple time scales, but its low resolution (0.5°) is not conducive to the study of drought patterns at the regional scale. Therefore, referring to the calculation method of SPEIbase, this study calculated the water deficit based on high-resolution PRE and PET data in China, fitted the water deficit data series using the Log-Logistic method, and used python tools to calculate SPEI data at 1~12 month time scales and 5 km spatial resolution for China. NDVI data are sourced from the MOD13A2 dataset provided by the US Geological Survey's Land Processes Distributed Active Archive Center, with a spatial resolution of 1 km and two images per month. To synchronize with SPEI data temporal scales, we applied the Maximum Value Composite (MVC) technique to generate monthly and annual NDVI data series. The vegetation cover data is derived from the MODIS land cover product MCD12Q1, which includes 17 major land cover types. To minimize the impact of vegetation cover changes on CED and LED analysis, our study was conducted only on pixels where no vegetation changes occurred between 2000 and 2022. Pixels with changes in vegetation cover were defined as non-vegetated areas. Subsequently, all raster datasets were resampled to a 5 km resolution to facilitate analysis and discussion.

Methods

The main including data sources, methodology, and results are shown in Fig. 2.

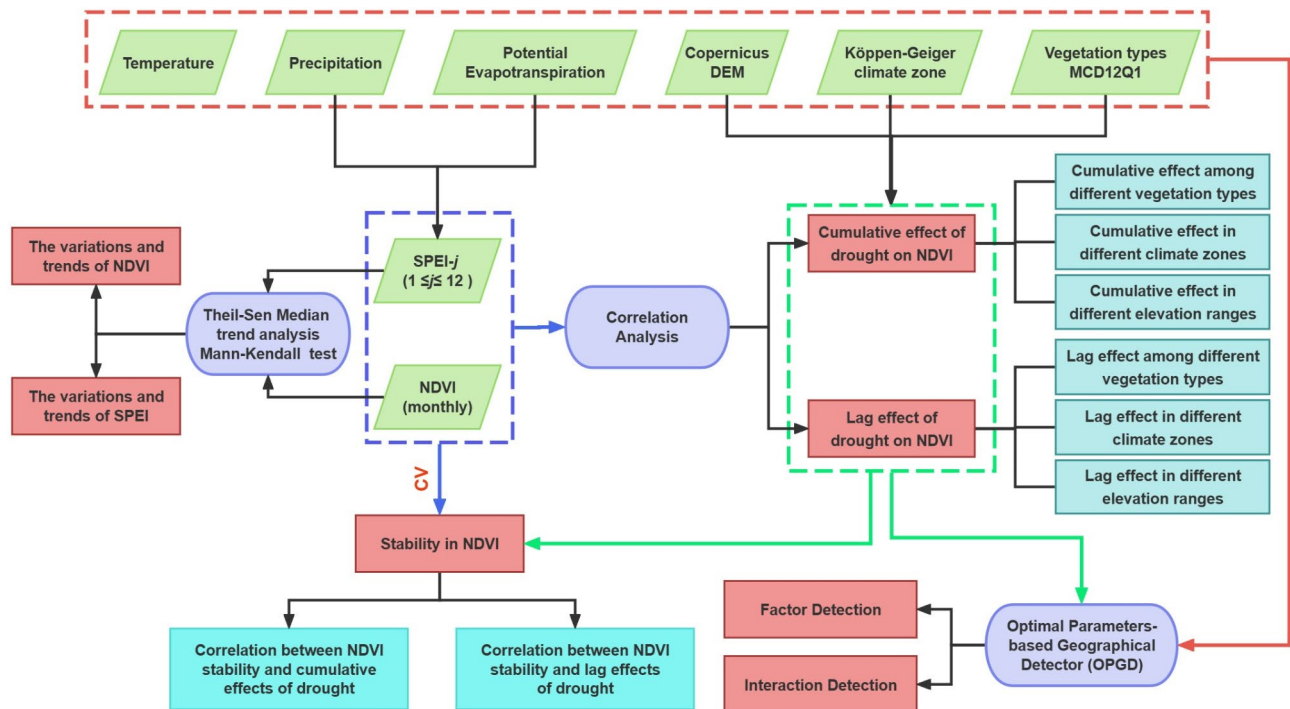


Fig. 2. The technical study designs.

Standardized precipitation evapotranspiration index (SPEI)

The SPEI is utilized to assess drought severity across various temporal scales. SPEI computation involves fitting the cumulative moisture deficit (D_i) series with an appropriate probability distribution function, followed by normalization to derive SPEI classes¹⁵. Negative SPEI values indicate water deficit, while positive values denote surplus moisture. D_i is accumulated based on monthly differences between PRE and PET, with the multi-temporal nature of SPEI derived from the variability in accumulated months i of D_i . Our study focuses on drought time scales ranging from 1 to 12 months ($i = 1, 2, \dots, 12$). In this research, we employed the log-logistic probability distribution function to fit D_i and conducted SPEI calculations for China using the gma library in Python. Compared to other commonly used meteorological drought indices, SPEI exhibits greater capability in measuring the impacts of drought on agricultural and ecological responses³⁷.

Theil-Sen median (TS) trend analysis and Mann-Kendall (MK) test

The TS method is a robust computational technique, free from parametric assumptions, utilized for trend analysis. Renowned for its computational efficiency and resilience to measurement inaccuracies and outliers, it is frequently employed in the analysis of lengthy time series datasets. The formula is outlined below:

$$\beta = \text{Median} \left(\frac{X_j - X_i}{j - i} \right), 2000 \leq i < j \leq 2022 \quad (1)$$

In the equation, X_j and X_i denote the time series data, with $\beta > 0$ signifying an upward trend and $\beta < 0$ indicating a downward trend.

The MK test is a non-parametric statistical method³⁸. Its inclusivity, which does not require measurement data to follow a normal distribution, linear trend, or be affected by missing and outlier values, has made it widely applied in significant trend testing of long time series data³⁹. In this study, TS and MK tests were employed to quantitatively analyze the trend changes and significance ($P < 0.05$) of SPEI and NDVI time series from 2000 to 2022.

Cumulated effects (CED) and lag effects of drought (LED)

We constructed NDVI time series data consisting of all 276 ($12 * 23 = 276$) monthly images from 2000 to 2022. Simultaneously, we created SPEI_j data sequences containing 276 images. Correlation analysis was performed on the two time-series, yielding the correlation coefficient R_{cum_j} between SPEI_j and NDVI at an accumulated time scale of j months at the pixel level. Thus, twelve correlation coefficients were obtained at each pixel location. Then, the optimal response month for CED and the corresponding cumulative intensity R_{cum_j} for each pixel were determined based on the maximum value ($R_{\text{max-cum}}$) under the significance level of $p < 0.05$ ⁴⁰. The calculation formula is as follows:

$$R_{\text{cum}_j} = \text{corr} (NDVI, SPEI_j), 1 \leq j \leq 12 \quad (2)$$

$$R_{max-cum} = \max (|R_{cum_j}|), 1 \leq j \leq 12 \quad (3)$$

In the equation, R_{cum_j} is the correlation coefficient between NDVI and SPEI_j, SPEI_j represents the drought index at a time scale of j months ($1 \leq j \leq 12$), and $R_{max-cum}$ is the absolute maximum value of R_{cum_j} .

Unlike the CED calculation, LED should only consider SPEI at a time scale of 1 month. We performed correlation analyses between the monthly NDVI time series spanning from 2000 to 2022 and the SPEI₁ sequence with various offsets (e.g., 0 months, 1 month, 12 months). Subsequently, 13 correlation coefficients were computed at each pixel location. Then, utilizing the maximum value, we identified the optimal response month for LED and its corresponding lag intensity R_{lag_i} for each pixel (referred to as $R_{max-lag}$), employing a significance level of $p < 0.05$ ³¹. The calculation formula is provided below:

$$R_{lag_i} = \text{corr} (NDVI, SPEI_1), 0 \leq i \leq 12 \quad (4)$$

$$R_{max-lag} = \max (|R_{lag_i}|), 0 \leq i \leq 12 \quad (5)$$

In the equation, R_{lag_i} is the correlation coefficient between NDVI and SPEI₁, where i represents the time scale of LED from 0 to 12 months. SPEI₁ denotes the SPEI at the one-month time scale, and $R_{max-lag}$ is the absolute maximum value of R_{lag_i} .

Optimal parameters-based geographical detector (OPGD) model

Spatial heterogeneity is a prevalent characteristic observed in the non-uniform distribution of spatial issues. Spatially stratified heterogeneity analysis studies the heterogeneity between explanatory variable layers by comparing intra-layer spatial variance and inter-layer spatial variance. The geographic detector model shows great potential in spatially stratified heterogeneity analysis. The factor detector can detect the explanatory power of each variable factor on the spatial variability of the dependent variable based on the size of the q value, while the interaction detector can identify the superimposed effects between different factors. Some studies have pointed out that in the use of geographic detectors, the discretization of continuous data may be subjectively influenced by the operator, which may compromise the effectiveness of the model. However, OPGD model optimizes the data discretization method, which can further extract the information contained in spatial explanatory variables⁴¹. To explore the impact of vegetation type, climate zones, and elevation on CED and LED, while considering the inclusion of temperature, precipitation, and potential evapotranspiration in the SPEI indicator, this study selects vegetation type data, climate data, DEM data, and temperature, precipitation, and potential evapotranspiration data as independent variables. The CED and LED intensities in drought lag effects are used as dependent variables. The OPGD model is employed to detect and analyze the driving factors behind the spatial differentiation of temporal effects.

Stability analysis

The coefficient of variation (CV) represents the degree of data dispersion, with its magnitude reflecting the proximity of sample points to the mean⁴². It is commonly used to assess the stability of time series data. In our investigation, we explored the influence of drought timing effects on the stability of NDVI by computing the CV for NDVI spanning from 2000 to 2022. The formula for calculating CV is as follows:

$$cv = \frac{\sigma}{\mu} \quad (6)$$

In the equation, cv represents the coefficient of variation, μ denotes the mean of NDVI, and σ represents the standard deviation.

Results

The variations and trends of NDVI and SPEI

During the last two decades, the annual average NDVI in China has significantly increased at a rate of 0.026/10a ($R^2 = 0.90$), rising from 0.584 to 0.640. Observing the changes in NDVI across different value ranges reveals that the increase in annual average NDVI stems from a decrease in the proportion of low-value NDVI and an increase in the proportion of high-value NDVI, with the most significant increase observed in the proportion of NDVI values above 0.8 (Fig. 3a). At the annual scale, the SPEI trend in the study area is not significant, fluctuating between -0.708 and 0.445 , showing an overall nonsignificant increasing trend of $0.17/10a$ ($R^2 = 0.10$) (Fig. 3b).

In order to delve deeper into the changing attributes of vegetation and drought within the study region, we utilized the TS-MK methodology to examine the spatial fluctuations in NDVI and SPEI from 2000 to 2022 (Fig. 3c, d, e, f). As shown in Fig. 3c, the range of annual NDVI trend changes in vegetated areas is mainly from -0.12 to $0.15/10a$, with 85.1% of the areas having a positive slope in NDVI. The MK test results indicate that the proportion of vegetated areas exhibiting significant upward trends (SUT), nonsignificant upward trends (NUT), nonsignificant downward trends (NDT), and significant downward trends (SDT) in NDVI are 53.5%, 31.6%, 12.6%, and 2.3%, respectively (Fig. 3d). Areas with SUT are mainly distributed in northeastern China, the Loess Plateau, the eastern Qinghai-Tibet Plateau, the southeastern Qaidam Basin, the southern Junggar Basin, the edge of the Tarim Basin, and areas south of the Yangtze River, while areas with SDT are mainly distributed in the North China Plain, the western Junggar Basin, the Sichuan Basin, and the southwestern Qinghai-Tibet Plateau. Figure 3e and f show the trends in SPEI, with the range of annual SPEI trend changes mainly from -1.2 to $0.9/10a$. Among vegetated areas, 34.8% have a negative SPEI slope. According to the MK test results, the proportions of vegetated areas exhibiting SUT, NUT, NDT, and SDT in SPEI are 16.0%, 49.2%, 29.3%, and

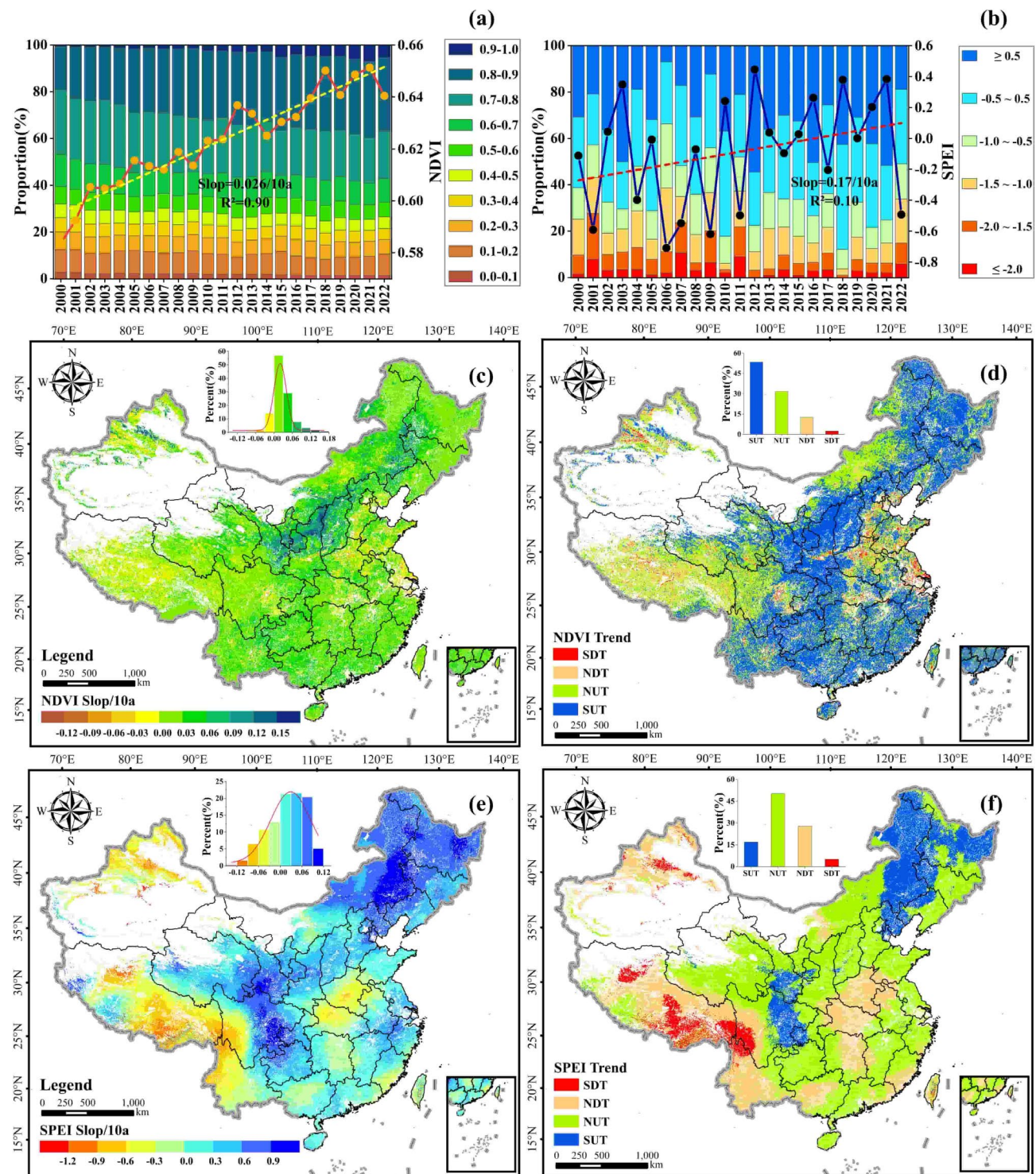


Fig. 3. Trends and distribution characteristics of NDVI and SPEI from 2000 to 2022. **(a)** Temporal changes of annual NDVI and proportions of NDVI in different value ranges. **(b)** Temporal changes of annual-scale SPEI and proportions of SPEI in different value ranges. **(c)** Spatial distribution of TS slopes for annual NDVI. **(d)** Spatial distribution of significance levels for annual NDVI. **(e)** Spatial distribution of TS slopes for annual SPEI. **(f)** Spatial distribution of significance levels for annual SPEI. (the maps are based on the standard map produced under the supervision of the Ministry of Natural Resources of the People's Republic of China: Approval number GS (2023) 2763, <http://bzdt.ch.mnr.gov.cn/>, created by ArcMap, version 10.8, <http://www.esri.com/>).

5.5%, respectively (Fig. 3f). The SUT region mainly encompasses the northeastern areas of China and the eastern Tibetan Plateau, whereas the SDT region is primarily distributed across the southern Junggar Basin and the southwestern Tibetan Plateau. Furthermore, subtle drought trends have been observed in the northwestern regions of China and the middle to lower sections of the Yangtze River. Over the past two decades, areas with improved vegetation growth in the study area correspond to areas with wetter drought conditions, occurring in northeastern China and the eastern Qinghai-Tibet Plateau, while areas with deteriorating vegetation growth correspond to areas with drier drought conditions, occurring in the southwestern Qinghai-Tibet Plateau and the southern Junggar Basin.

Drought's cumulative effect on NDVI (CED)

The spatial distribution characteristics of drought's cumulative effect on NDVI

The spatial distribution of CED intensity and the corresponding CED months across the study area are shown in Fig. 4. The impact of CED on vegetation growth is notable, demonstrated by the presence of CED in 35.94% of vegetated areas, all of which passed the significance test ($p < 0.05$). In these regions showing significant correlations, 77.44% of the areas exhibited a positive correlation between SPEI and NDVI. These sites are predominantly situated in the Loess Plateau, Sichuan Basin, southeastern hills, western Qinghai-Tibet Plateau, and the periphery of the Tarim Basin. Conversely, adverse correlations are primarily found in the northeastern and southwestern regions of the Qinghai-Tibet Plateau (Fig. 4a).

There is evident spatial heterogeneity in the response of vegetation NDVI to CED (Fig. 4b), with an average CED of 5.56 months. Among these, short-term droughts (2–4 months) have the largest impact on vegetation, affecting up to 53.60% of the area, primarily distributed in the northeast and Loess Plateau regions. Additionally, long-term cumulative droughts (12 months) also account for a considerable proportion (16.27%).

The performance of cumulative effects varies across different vegetation types (VT)

The discrepancies in CED among various vegetation types were investigated (Fig. 5a). The longest CED duration is observed in grassland, with an average of 5.90 months, followed by cropland (5.36 months), shrubland (5.32 months), and forest (4.72 months). As the height of the vegetation canopy increases, the impact of drought on NDVI CED gradually decreases. Among the secondary classifications of vegetation types, croplands and natural vegetation mixtures (CNVM) have the longest CED duration (8.27 months), while deciduous broadleaf forests (DBF) have the shortest CED duration (3.54 months).

The performance of cumulative effects varies across different climatic zones (CZ)

Based on Köppen-Geiger climate type data, we analyzed the response of NDVI to cumulative droughts in different climatic zones (Fig. 5b). Viewed through the lens of climatic zones, the Cold (temperate, sub-frigid) climatic zone exhibits the lowest average CED of 4.13 months, while the Temperate and Arid climatic zones have relatively higher and similar average CEDs, at 6.91 months and 6.77 months, respectively. The Tropical climatic zone has an average CED of 5.50 months, and the ET (polar) climatic zone has an average CED of 4.82 months. Among the subtypes of climate types, the maximum CED time appears in Cwa (7.67 months), while the minimum is in Dwb (3.80 months).

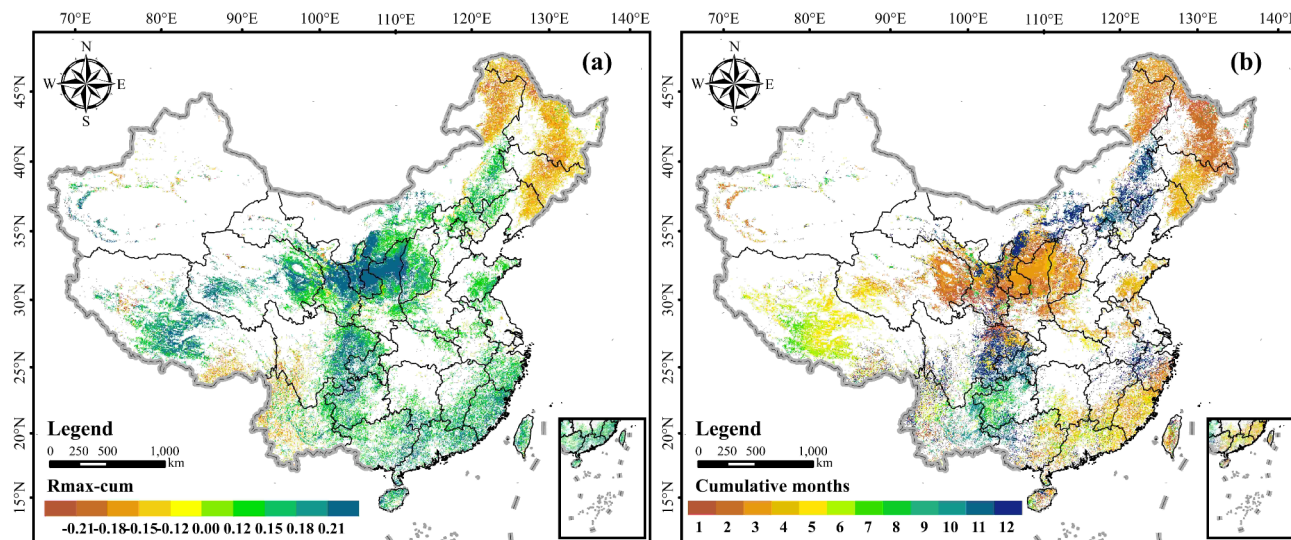


Fig. 4. (a) Spatial distribution of $R_{\text{max-cum}}$ and (b) cumulative months. (the maps are based on the standard map produced under the supervision of the Ministry of Natural Resources of the People's Republic of China: Approval number GS (2023) 2763, <http://bzdt.ch.mnr.gov.cn/>, created by ArcMap, version 10.8, <http://www.esri.com/>).

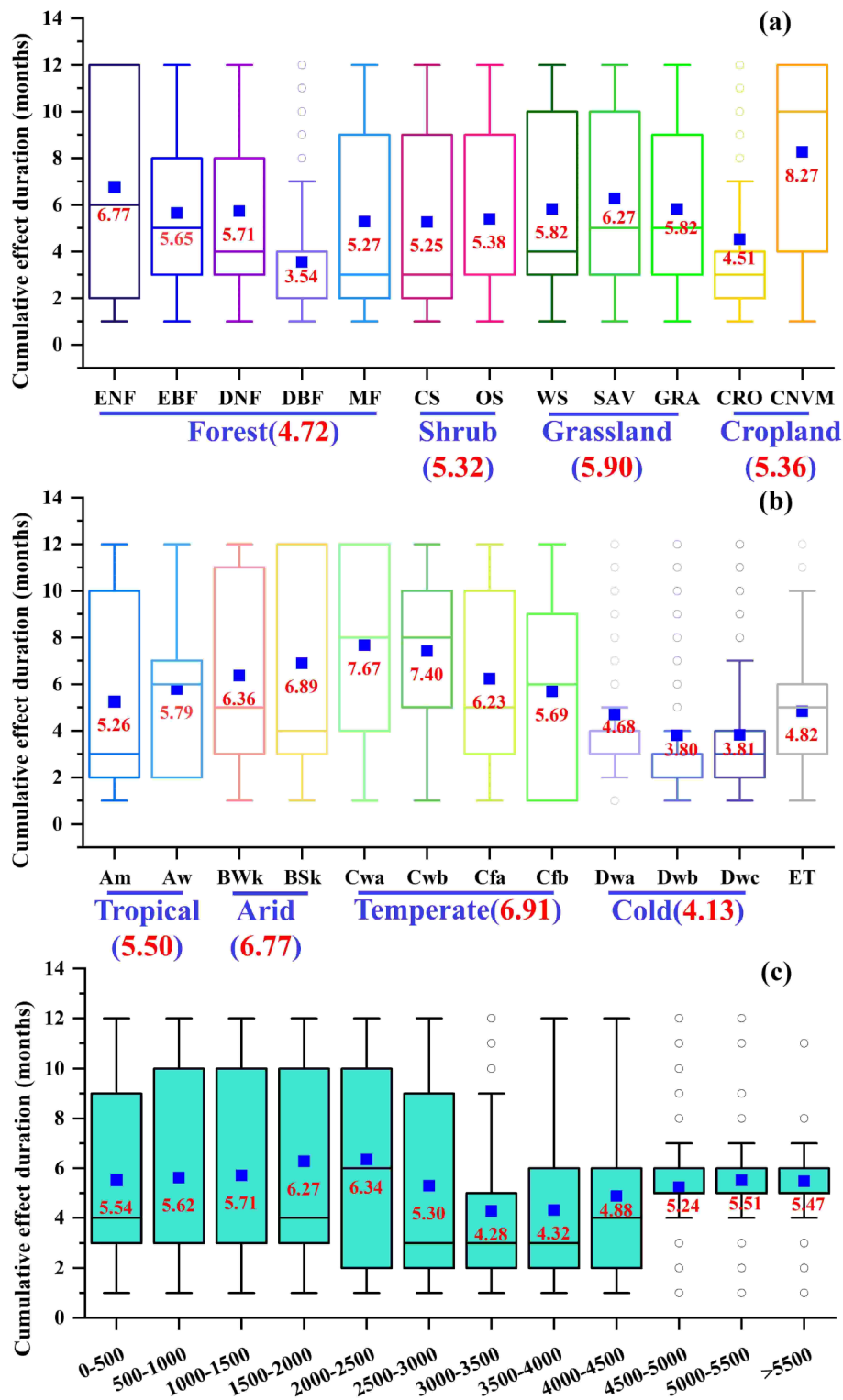


Fig. 5. (a) CED on different vegetation types; (b) CED on different climatic zones; (c) CED on different elevations.

The performance of cumulative effects in different elevation ranges

To investigate the differences in CED along an elevation gradient, we reclassified elevation into twelve categories with intervals of 500 m. The average cumulative months of vegetation NDVI response to drought show a slow increase with elevation up to 2500 m, followed by a rapid decrease between 2500 m and 3500 m, and then a slow increase again for elevations above 3500 m (Fig. 5c). The range of CED months varies between 4.28 and 6.34

months across different elevation levels. We found the maximum CED months in the elevation range of 2000 to 2500 m (6.34) and the minimum in the range of 3000 to 3500 m (4.28).

The lag effects of drought on NDVI (LED)

The spatial distribution characteristics of the lag effects of drought on NDVI

Utilizing pixel-scale $R_{\text{max-lag}}$ calculations, we derived the spatial distribution of LED intensity and LED months within the study area (Fig. 6). Compared to CED, LED demonstrates a broader influence on NDVI (significant correlation area covering 39.22% of vegetated area, $p < 0.05$). Specifically, 67.29% of vegetated regions exhibit significantly enhanced NDVI due to lagged drought, while 32.71% of areas show a negative impact on NDVI from SPEI. This adverse effect is primarily concentrated in the northeastern region, northwestern part of the North China Plain, western and central parts of the Qinghai-Tibet Plateau, and northern part of the Tarim Basin (Fig. 6a).

The average lagged effect time in the study area is 6.42 months, with the largest affected area observed for droughts with a lag of 10 months (covering 13.98% of the affected area). This is followed by droughts with a lag of 1 month (13.14%) and 11 months (11.57%). Droughts with a lag of 10 to 12 months account for 33.36% of all lagged periods, mainly concentrated in the Loess Plateau region. They exhibit a spatial distribution pattern of drought lagged effects centered around the Loess Plateau, gradually decreasing towards the surrounding areas (Fig. 6b).

The performance of lag effects varies among different vegetation types (VT)

The manifestation of LED in different vegetation types due to drought is illustrated in Fig. 7a. Vegetation types with longer lagged times from largest to smallest are grassland (7.72 months), cropland (7.37 months), forest (6.78 months), and shrubland (6.48 months). We observed both the longest and shortest lagged effects within the secondary classification of grassland types, with grassland exhibiting the longest lagged effect (8.46 months) and sparse grassland showing the shortest lagged effect (6.22 months).

The manifestation of lag effects varies across different climatic zones (CZ)

In different climate zone areas, the lagged response of vegetation NDVI to drought is shown in Fig. 7b. There are notable differences in the lagged effects across climate zones, with the maximum lagged effect occurring in the Arid climate zone (8.35 months) and the minimum lagged effect occurring in the Tropical climate zone (4.82 months). Additionally, the ET (Polar), Cold (Temperate, Subpolar), and Temperate (Subtropical) zones exhibit lagged effects of 7.87 months, 7.27 months, and 7.04 months, respectively. Within the subtypes of climate types, the maximum lagged effect occurs in the Bsk subtype (8.89 months), while the minimum occurs in the Aw subtype (3.50 months).

The performance of lagged effects in different altitude ranges

We statistically analyzed the distribution pattern of LED months based on established elevation gradient intervals (Fig. 7c). Along the elevation gradient, the lagged effects show a pattern of initially increasing (0~1500 m), then decreasing (1500~2500 m), followed by another increase (2500~3500 m), then decrease (3500~5000 m),

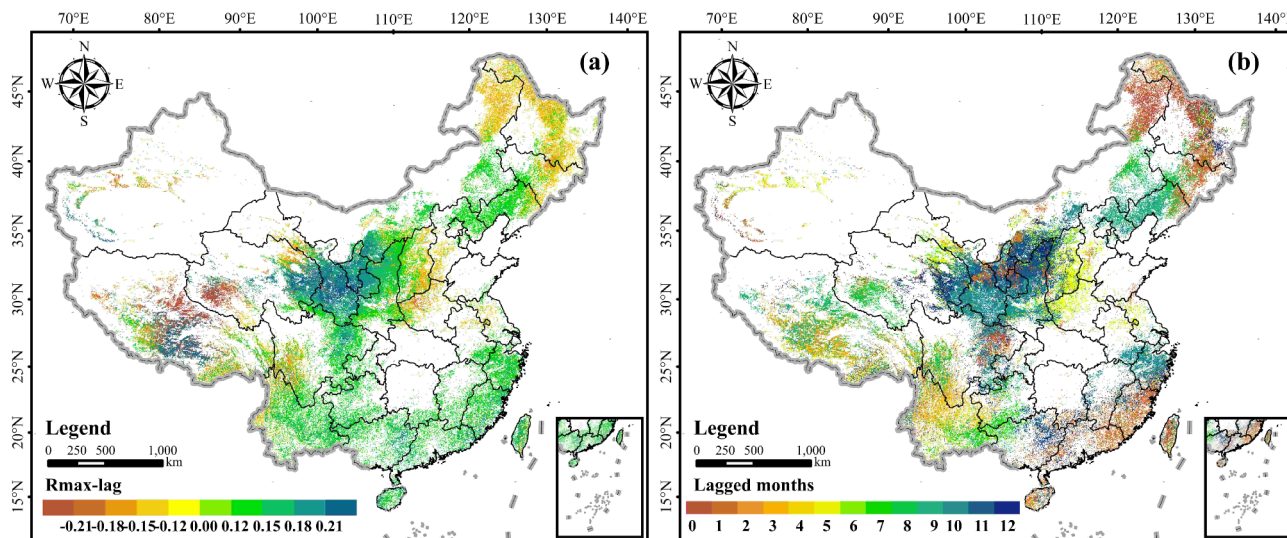


Fig. 6. (a) Spatial distribution of $R_{\text{max-lag}}$ and (b) lagged months. (the maps are based on the standard map produced under the supervision of the Ministry of Natural Resources of the People's Republic of China: Approval number GS (2023) 2763, <http://bzdt.ch.mnr.gov.cn/>, created by ArcMap, version 10.8, <http://www.esri.com/>).

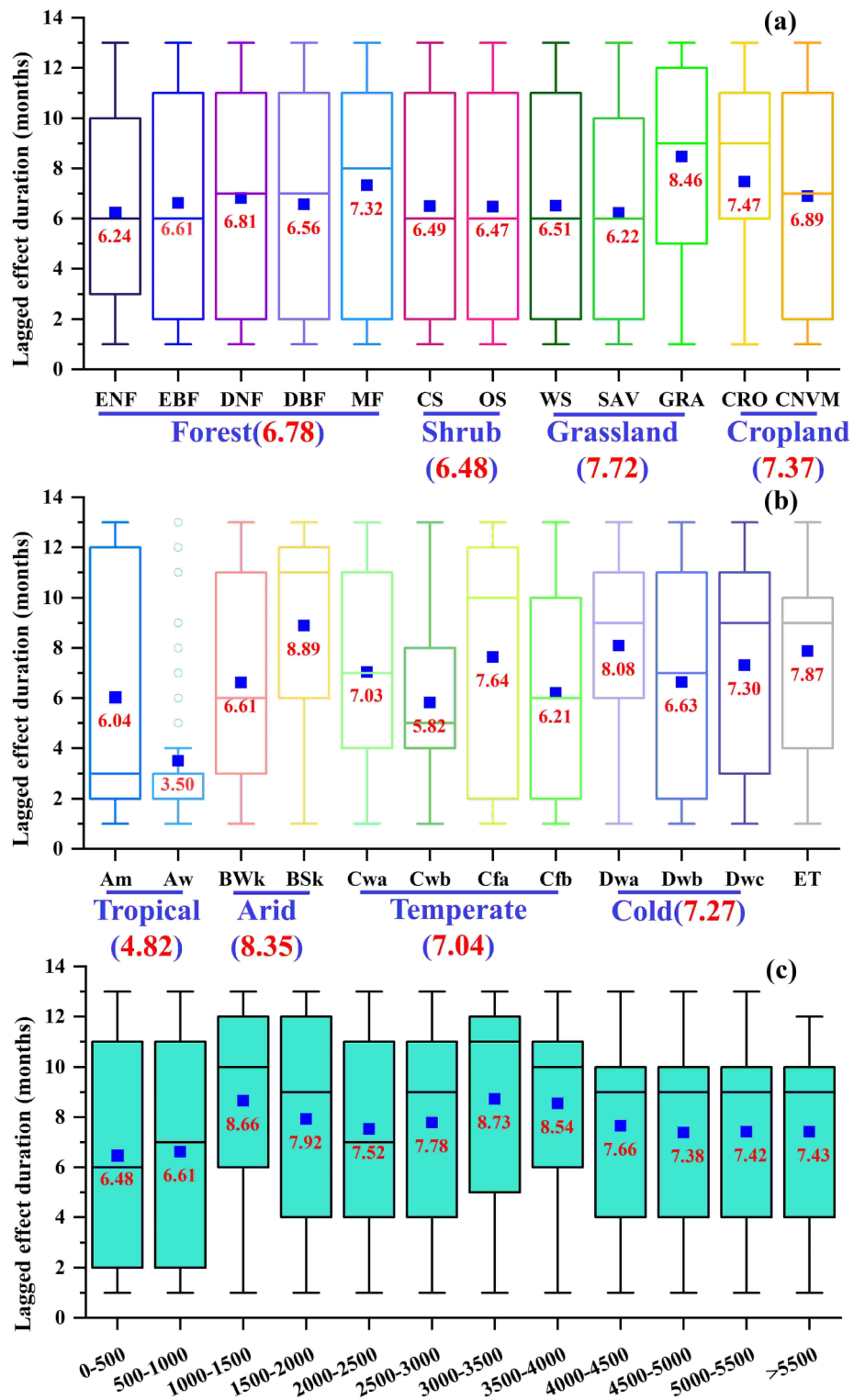


Fig. 7. (a) LED on different vegetation types; (b) LED on different climate zones; (c) LED on different elevations.

and finally stabilizing (> 5000 m). The maximum and minimum lagged months occur in the intervals of 3000~3500 m (8.73 months) and 0~500 m (6.48 months), respectively.

Analysis of the driving factors of drought-induced NDVI temporal effects

We used the OPGD model to further quantify the explanatory power of single-factor effects and two-factor interactions on CED and LED. The explanatory power of each factor on the intensity of CED and LED is shown

in Fig. 8a. For CED, climate type ($q=0.269$) and potential evapotranspiration ($q=0.259$) dominate as the driving factors, while the explanatory power of vegetation type ($q=0.213$) is also considerable, followed by temperature ($q=0.199$) and precipitation ($q=0.180$), with elevation factor contributing the least ($q=0.085$); with the dominant driving factors for LED are temperature ($q=0.173$) and potential evapotranspiration ($q=0.167$), followed by climate type ($q=0.118$), elevation ($q=0.095$), precipitation ($q=0.076$), and vegetation type ($q=0.026$). From the perspective of single-factor driving force on temporal lag effects, elevation and temperature contribute similarly to the intensity of CED and LED. However, compared to LED, precipitation, potential evapotranspiration, climate type, and vegetation type have a stronger explanatory power on the intensity of CED. In our investigation into the interactive effects of multiple factors on the temporal impact of drought, we consistently noted a significant trend: with all fifteen combinations of dual-factor interactions contribute substantially to the enhanced explanatory capacity of the dependent variable. Specifically, in the analysis of CED intensity interactions, two combinations demonstrate a dual-factor augmentation effect, while thirteen combinations exhibit nonlinear augmentation effects (Fig. 8b). In the examination of LED intensity interactions, six combinations manifest dual-factor augmentation effects, and nine combinations display nonlinear augmentation effects (Fig. 8c).

Discussion

The cumulative and lagged effects of drought on vegetation NDVI

To study the impact of drought on the CED of NDVI under long-term hydrothermal conditions, we analyzed the differences in CED across various sub climatic zones based on the Köppen-Geiger climate classification. In the Tropical zone, where precipitation during the driest months (P_{dry}) is the key sub-classification factor, the average CED duration increases as P_{dry} decreases (Am: 5.50 months, Aw: 5.79 months). This indicates that as precipitation decreases, soil moisture gradually depletes, leading to slower vegetation recovery and prolonged drought impacts. In contrast, in the Arid zone, where the key sub-classification factor is the mean annual precipitation (MAP), the average CED duration decreases as MAP decreases (BSk: 6.89 months, BWk: 6.36 months). Vegetation in Arid zones, which has long adapted to extreme drought conditions, has a stronger rapid response and recovery mechanism, resulting in shorter drought impact durations. In the Temperate zone, when temperature conditions are not considered, further classification by annual precipitation distribution shows that the more evenly distributed the precipitation is throughout the year, the shorter the CED duration (Cwa and Cwb: 7.54 months, Cfa and Cfb: 5.96 months). Even precipitation provides continuous water supply to vegetation, reducing the adverse effects of prolonged drought on vegetation health. Moreover, under the same annual precipitation distribution, regions with lower average temperatures in the hottest months have shorter CED durations (Cwb < Cwa, Cfb < Cfa, Dwc ≈ Dwb < Dwa). Lower temperatures reduce transpiration, preserving more soil moisture and mitigating the drought's impact on vegetation. Long-term hydrothermal conditions also significantly influence the LED on NDVI. When considering only long-term water conditions, in the Tropical zone, the LED duration shortens as P_{dry} decreases (Am: 6.04 months, Aw: 3.50 months). Reduced water availability causes vegetation to respond quickly, shortening the drought lag effect duration. Similarly, in the Arid zone, as MAP decreases, the LED duration also shortens (BSk: 8.89 months, BWk: 6.61 months), further confirming the sensitivity and rapid response of vegetation to water resource changes in arid regions. In the Temperate zone, where temperature conditions are not considered, the climate is classified into winter-dry (Cwa, Cwb) and no-dry-season (Cfa, Cfb) zones. The average LED time in winter-dry zones (6.43 months) is shorter than in no-dry-season zones (6.93 months). Vegetation in winter-dry zones has stronger adaptation to drought, which reduces the LED duration. Further analysis of long-term temperature conditions shows that in the Temperate zone, as the temperature in the hottest month of the year decreases, the LED duration also shortens (Cwa and Cfa: 7.34 months, Cwb and Cfb: 6.02 months), indicating that lower temperatures can mitigate the drought effects. In the Cold zone, the subcategory with the highest average temperature in the hottest month, Dwa, has a longer LED duration (8.08 months) compared to Dwb (6.63 months) and Dwc (7.30 months). Higher temperatures increase transpiration, depleting more water and exacerbating the drought impact. However, no such pattern was observed between Dwb and Dwc, likely due to the influence of other environmental factors.

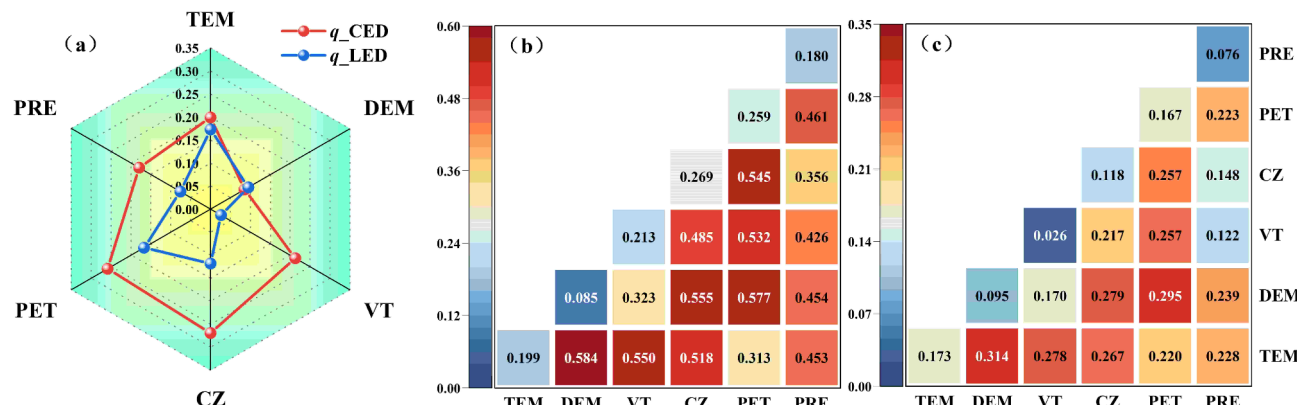


Fig. 8. Results of the analysis on the driving factors of temporal lag effects. (a) Radar chart of the q-values for each influencing factor. (b) Heatmap of CED interaction detector. (c) Heatmap of LED interaction detector.

The variability in time effects reflects different vegetation response strategies to drought⁴³. In times of drought stress, plant roots react to fluctuations in soil moisture at both cellular and whole root structural levels. Root morphology undergoes alterations to augment water uptake efficiency under conditions of water scarcity, a phenomenon originating from coordinated cell division, elongation, and differentiation at the root tip⁴⁴. The average cumulative effect time for grasslands was 5.90 months, which is similar to studies on CED in global (5.28 months) and Central Asian (6.72 months)^{28,40}. However, the average cumulative effect time for forests is only 4.72 months, which contrasts with previous research. Zhou, et al.⁴⁵ found that forests, due to their deeper roots and stronger access to groundwater, are more resistant to cumulative drought. To explore this further, we analyzed the proportions of different vegetation types in different cumulative months and their cumulative effect intensities (see Fig. 9a). Forests showed a relatively larger proportion in cumulative effect times of 2 months (31.8%) and 3 months (19.9%), primarily distributed in the Cold climate zone of Northeast China (Fig. 4b). Influenced by the Asian high pressure and the East Siberian Mountains, the Northeast region of China experiences long, cold, and dry winters, with short spring and autumn seasons and an average annual temperature of approximately 3 °C, making it the region with the lowest annual average temperature in China after the Qinghai-Tibet Plateau. Drought is often accompanied by high temperatures and low precipitation. Increased temperatures lead to the release of soil moisture from frozen soil, prompting rapid plant responses, while abundant precipitation during wet periods can cause frost damage under severe cold conditions, resulting in leaf damage and shedding. It is these reasons that contribute to the unusual drought tolerance of forests in the Northeast region, leading to a negative correlation between forests and SPEI under conditions of 2 and 3 months cumulative effect times. Our study also identified the lag effect durations of various vegetation types during drought as follows: Grassland>Cropland>Forest>Shrub. While previous research has interpreted the duration of lag effect as indicative of vegetation sensitivity to drought, our study proposes that evaluating vegetation sensitivity to drought based solely on lag effect duration, without accounting for its intensity, may be inappropriate. In Fig. 9b, we observed a significant negative correlation between grasslands and drought, with these negative correlations mainly occurring in the Qinghai-Tibet Plateau region (Fig. 6a). Despite whether the impact is positive or negative, the absolute value of grassland lag effect correlations is generally the highest compared to other vegetation types in most months, indicating a stronger response of grasslands to lagging drought (i.e., higher sensitivity). Longer lag effect times imply that vegetation is more likely to be affected by the lingering effects of previous months' droughts and is less likely to recover from earlier droughts, which corroborates the findings of our study regarding the longest lag effect time observed for grasslands⁴⁶.

The vertical zonation of altitude profoundly influences vegetation response to climate change⁴⁶. In general, with increasing altitude, temperatures decrease gradually while precipitation levels rise⁴⁷. Decreasing temperature slows down vegetation vitality, while increasing precipitation promotes vegetation growth. This bidirectional interaction makes the impact of altitude on vegetation more complex, especially under arid conditions. The time effect of drought on vegetation NDVI shows similarity along the altitude gradient, with fluctuations in cumulative months and lag months in mid-low altitude areas and stability in high altitude areas. Notable variations in drought conditions exist across varying altitudes, particularly noticeable in mid-low altitude regions. These areas, characterized by intense human activities such as overgrazing and land use alterations, significantly affect vegetation ecosystems⁴⁸, resulting in considerable fluctuations in response to drought. As the altitude gradient increases, vegetation disturbance by human activities decreases, and drought conditions tend to stabilize, resulting in smaller monthly variations in vegetation NDVI response to drought. In high altitude areas, where precipitation is abundant, temperatures are low, rainfall variation is small, evapotranspiration is low, and soil moisture is sufficient. Ordinary droughts do not induce substantial alterations to vegetation habitats or impact their growth status significantly⁴⁹.

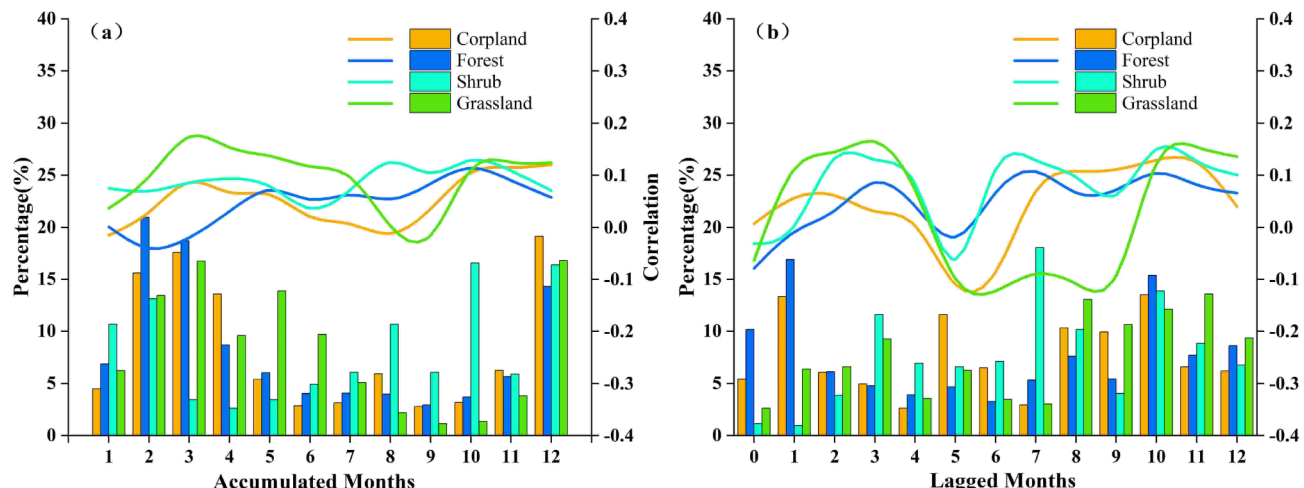


Fig. 9. Proportion of CED months and variations in CED intensity for different vegetation types (a); Proportion of LED months and variations in LED intensity for different vegetation types (b).

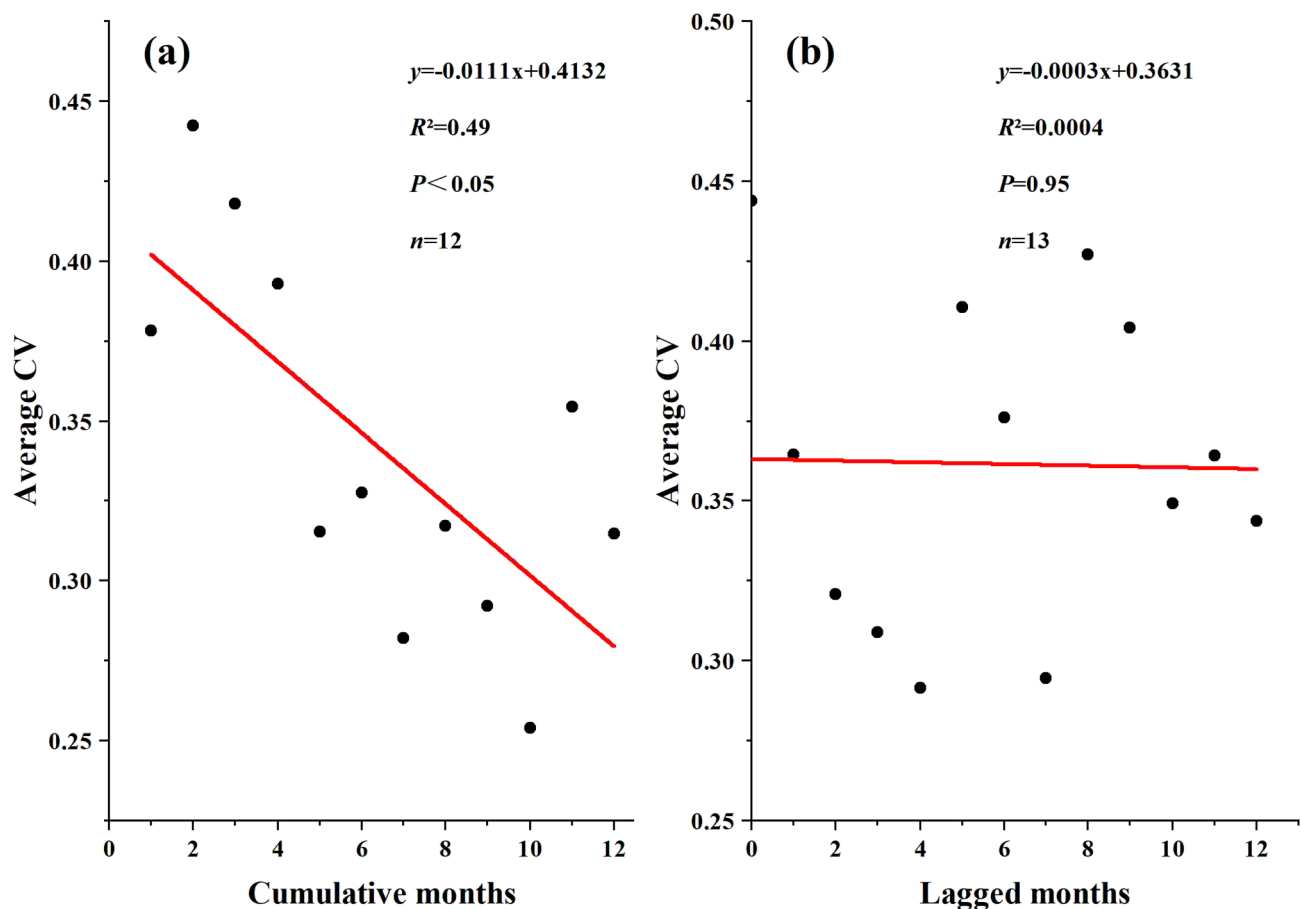


Fig. 10. (a) The relationship between CV and cumulative months. (b) The relationship between CV and lag months.

Overall, vegetation's asymmetric temporal response to drought is influenced by complex environmental factors⁵⁰. To better understand the underlying mechanisms of vegetation's response to drought, we used the OPGD model's factor detector and interaction detector to analyze the drivers of lagged effects. We found that the contribution rates to CED and LED intensity, from highest to lowest, were CZ > PET > VT > TEM > PRE > DEM for CED, and TEM > PET > CZ > DEM > PRE > VT for LED. We also observed that the interaction of two factors significantly enhanced the effect on the lagged response (Fig. 8a, b, c). As discussed, vegetation's response to drought is influenced by both drought development mechanisms and physiological factors. During drought, it suppresses nutrient flow by reducing soil moisture availability and hindering the contact between roots and soil nutrients, limiting vegetation's absorption of water and nutrients, thus affecting growth⁵¹. Long-term high temperatures and low precipitation exacerbate evapotranspiration losses from surface soil moisture⁵². Plants have also evolved drought-resistant strategies to prevent water loss, balance optimal water supply to key organs, maintain cell water content, and survive drought conditions^{25,44}.

The stability of vegetation NDVI is related to the duration of cumulative effects

The stability of vegetation growth status is frequently impacted by various natural disasters⁵³, with drought often emerging as the most prevalent and severe. This study highlights the widespread occurrence of cumulative and lag effects of drought on vegetation. The asymmetric time-effect response of vegetation to drought is influenced by unique combinations of climatic conditions, altitude gradients, and vegetation characteristics specific to each climatic zone, determining the differences in vegetation tolerance and sensitivity to drought^{28,54}. This study further examined whether these distinctions directly correlate with the stability of vegetation NDVI by assessing the effect of drought on vegetation stability across various cumulative and lag months using the CV. Figure 10 demonstrates a significant decrease in CV with rising cumulative months ($R^2 = 0.49$, $p < 0.05$) (Fig. 10a), whereas the correlation between lag months and CV appears relatively minor and non-significant (Fig. 10b). This suggests that the stability of vegetation NDVI exhibits a more substantial response to the disturbance of CED.

Studies have shown that compared to short-term droughts, long-term droughts may lead to greater variability in vegetation growth. Some research suggests that after experiencing common short-term droughts, vegetation can maintain its original system structure and function based on its regulatory capacity. However, long-term droughts may prevent vegetation from fully recovering to previous levels, resulting in a positive correlation between vegetation stability and cumulative drought months. Other studies have indicated that

vegetation growth responses to different degrees of drought can be summarized into low-response and high-response stages. In the low-response stage, when soil moisture is slightly deficient, vegetation growth resistance to drought is high, resulting in a lower frequency of vegetation growth response to drought. In the high-response stage, when moisture deficiency exceeds the drought threshold, vegetation growth resistance to drought rapidly declines, leading to a rapid increase in the frequency of vegetation growth response to drought. Since 2000, drought events in China have developed rapidly, usually reaching severe drought levels within weeks and lasting for relatively short durations, mostly between 15 and 60 days. Under such intense drought conditions, vegetation resistance quickly diminishes, severely impacting vegetation growth stability. However, long-term droughts often develop slowly, with milder drought intensities. Under these conditions, vegetation has more space to exert resistance below the drought threshold and gradually adapt to drought conditions. Although this resistance cannot completely offset the damage caused by drought, it can significantly mitigate the magnitude of vegetation growth stability changes. Therefore, this study suggests that short-term severe droughts have a more significant impact on vegetation growth stability.

Limitations

Although this study analyzed the characteristics of vegetation and drought changes in China and explored the temporal effects of drought on vegetation growth from multiple perspectives, there remains some uncertainty. Firstly, SPEI represents meteorological drought and cannot reflect soil moisture deficit changes. Pre-existing soil moisture can sustain normal vegetation growth during drought periods, adding to the uncertainty of the temporal effects of drought on vegetation growth. Secondly, the correlation analysis methods may lead to the loss of information about the nonlinear relationship between vegetation and drought. Additionally, we did not consider the impacts of other extreme climate events (such as heavy rain and floods), human activities (such as grazing and irrigation), or natural disturbances (such as pests) on vegetation growth⁵⁰. Future research can utilize machine learning methods to establish a more systematic regression model between soil moisture indicators, SPEI, and NDVI to further compare and analyze the impacts of drought. Moreover, more explanatory causal inference methods can be employed to study more complex influencing factors from extreme climate, human activities, and natural factors, providing a more scientific, reasonable, comprehensive, and holistic revelation of the interrelationship between drought and vegetation ecosystems.

Conclusions

This study analyzes the trends of vegetation and drought in China from 2000 to 2022, based on multi-time scale SPEI and NDVI data. It explores the cumulative and lagged effects of drought on NDVI, as well as their variations with vegetation type, climate zone, and elevation gradients. The main conclusions are as follows:

1. Over the past two decades, 85.1% of regions are becoming greener, with an overall NDVI increase rate of 0.026 per decade. Annual drought levels fluctuate over the years, with increasingly severe drought conditions in parts of southwestern and northwestern China.
2. The CED effect of drought significantly impacted 35.94% of vegetated areas, with 77.44% of these regions showing a positive correlation between SPEI and NDVI. Grasslands exhibited the longest CED (5.90 months), while forests had the shortest (4.72 months). In climate zones, the Temperate and Arid zones had higher average CEDs (6.91 and 6.77 months, respectively). The highest CED (6.34 months) was found at altitudes of 2000–2500 m, and the lowest (4.28 months) at 3000–3500 m.
3. The LED effect of drought significantly affected 39.22% of vegetated areas, with an average LED time of 6.42 months, which is longer than the average CED (5.56 months). Grasslands had the longest LED (7.72 months), while forests (6.78 months) and shrubs (6.48 months) had shorter LED durations. In climate zones, the Arid zone had the longest LED (8.35 months), and the Tropical zone the shortest (4.82 months). At different elevations, LED was smallest in the 0–500 m range (6.48 months).
4. Climate type and potential evapotranspiration were the dominant factors driving CED, contributing 0.269 and 0.259, respectively. For LED, temperature and potential evapotranspiration were the primary drivers (0.173 and 0.167). Interaction effect analysis showed that the combination of two factors significantly increased the impact on lagged effect intensity.
5. The study also found a significant negative correlation between vegetation NDVI stability and the duration of cumulative effects. Short-term, high-intensity droughts caused more severe damage to vegetation stability.

This study highlights the differences in the cumulative and lagged effects of drought on vegetation across different environmental factors, enhancing our understanding of how vegetation responds to drought and its mechanisms, providing scientific guidance for more effective ecological protection and management.

Data availability

All data included in this study are available upon request by contacting the corresponding author.

Received: 15 July 2024; Accepted: 14 February 2025

Published online: 21 February 2025

References

1. Liu, L. et al. Soil moisture dominates dryness stress on ecosystem production globally. *Nat. Commun.* **11**(1), 4892 (2020).
2. Kuwayama, Y., Thompson, A., Bernknopf, R., Zaitchik, B. & Vail, P. Estimating the impact of drought on agriculture using the U.S. drought monitor. *Am. J. Agric. Econ.* **101**, 193–210 (2019).

3. Vicente-Serrano, S. M. et al. Response of vegetation to drought time-scales across global land biomes. *Proc. Natl. Acad. Sci. U.S.A.* **110**(1), 52–57 (2013).
4. Xu, C. et al. Increasing impacts of extreme droughts on vegetation productivity under climate change. *Nat. Clim. Change.* **9**(12), 948–953 (2019).
5. Rigden, A. J., Mueller, N. D., Holbrook, N. M., Pillai, N. & Huybers, P. Combined influence of soil moisture and atmospheric evaporative demand is important for accurately predicting US maize yields. *Nat. Food* **1**(2), 127–133 (2020).
6. Park, S., Im, J., Park, S. & Rhee, J. Drought monitoring using high resolution soil moisture through multi-sensor satellite data fusion over the Korean peninsula. *Agric. For. Meteorol.* 237–238 (2017).
7. IPCC. Climate Change : Synthesis Report (Full Volume) Contribution of Working Groups I, II and III to the Sixth Assessment Report of the Intergovernmental Panel on Climate Change. (2023). <https://doi.org/10.59327/IPCC/AR6-9789291691647> (2023).
8. Yang, Z. et al. Decreased precipitation in the late growing season weakens an ecosystem carbon sink in a semi-arid grassland. *J. Appl. Ecol.* **58**(10), 2101–2112 (2021).
9. Peng, J., Wu, C., Zhang, X. & Wang, X. Satellite detection of cumulative and lagged effects of drought on autumn leaf senescence over the Northern Hemisphere. *Glob. Change Biol.* **25**, 2174–2188 (2019).
10. Cao, S. et al. Effects and contributions of meteorological drought on agricultural drought under different climatic zones and vegetation types in Northwest China. *Sci. Total Environ.* **821** (2022).
11. Li, Y. et al. Spatiotemporal heterogeneity in meteorological and hydrological drought patterns and propagations influenced by climatic variability, LULC change, and human regulations. *Sci. Rep.* **14**(1), 5965 (2024).
12. Zhang, X. et al. Drought propagation under global warming: Characteristics, approaches, processes, and controlling factors. *Sci. Total Environ.* **838**, 156021 (2022).
13. Guttman, N. B. Accepting the standardized precipitation index: a calculation algorithm. *J. Am. Water Resour. Assoc.* **35**(2), 311–322 (1999).
14. Newman, J. E. & Oliver, J. E. Palmer Index/Palmer Drought Severity Index. In *Encyclopedia of World Climatology* (ed Oliver, J.E.) 571–573 (Springer Netherlands, Dordrecht, 2005). https://doi.org/10.1007/1-4020-3266-8_159.
15. Vicente-Serrano, S., Beguería, S. & López-Moreno, J. I. A multiscale drought index sensitive to global warming: the standardized precipitation evapotranspiration index. *J. Clim.* **23**, 1696–1718 (2010).
16. Gumus, V. Evaluating the effect of the SPI and SPEI methods on drought monitoring over Turkey. *J. Hydrol.* **626**, 130386 (2023).
17. Meseguer-Ruiz, O. et al. Comparing SPI and SPEI to detect different precipitation and temperature regimes in Chile throughout the last four decades. *Atmos. Res.* **297**, 107085 (2024).
18. Wu, H., Svoboda, M. D., Hayes, M. J., Wilhite, D. A. & Wen, F. Appropriate application of the standardized precipitation index in arid locations and dry seasons. *Int. J. Climatol.* **27** (1), 65–79 (2007).
19. Guo, H. et al. Space-time characterization of drought events and their impacts on vegetation in Central Asia. *J. Hydrol.* **564**, 1165–1178 (2018).
20. Yuan, B. et al. Quantifying the drought sensitivity of vegetation types in northern China from 1982 to 2022. *Agric. For. Meteorol.* **359**, 110293 (2024).
21. Ma, M., Wang, Q., Liu, R., Zhao, Y. & Zhang, D. Effects of climate change and human activities on vegetation coverage change in northern China considering extreme climate and time-lag and -accumulation effects. *Sci. Total Environ.* **860**, 160527 (2023).
22. Scheiter, S. et al. Climate change promotes transitions to tall evergreen vegetation in tropical Asia. *Glob. Change Biol.* **26**(9), 5106–5124 (2020).
23. Wei, X. et al. Global assessment of lagged and cumulative effects of drought on grassland gross primary production. *Ecol. Ind.* **136**, 108646 (2022).
24. Frank, D. A. et al. Effects of climate extremes on the terrestrial carbon cycle: Concepts, processes and potential future impacts. *Glob. Change Biol.* **21**(8), 2861–2880 (2015).
25. Salazar-Tortosa, D. et al. The isohydric trap: a proposed feedback between water shortage, stomatal regulation, and nutrient acquisition drives differential growth and survival of European pines under climatic dryness. *Glob. Change Biol.* **24**(9), 4069–4083 (2018).
26. McDowell, N. et al. Mechanisms of plant survival and mortality during drought: Why do some plants survive while others succumb to drought? *New Phytol.* **178**(4), 719–739 (2008).
27. Wen, Y. et al. Cumulative effects of climatic factors on terrestrial vegetation growth. *J. Geophys. Res.: Biogeosci.* **124**(4), 789–806 (2019).
28. Liu, L. et al. Cumulative effects of drought have an impact on net primary productivity stability in central Asian grasslands. *J. Environ. Manag.* **344**, 118734 (2023).
29. Rogiers, N., Conen, F., Forger, M., Stöckli, R. & Eugster, W. Impact of past and present land-management on the C-balance of a grassland in the Swiss Alps. *Glob. Change Biol.* **14** (2008).
30. Zhang, Y. et al. A global moderate resolution dataset of gross primary production of vegetation for 2000–2016. *Sci. Data.* **4**(1), 170165 (2017).
31. Zhao, A., Yu, Q., Feng, L., Zhang, A. & Pei, T. Evaluating the cumulative and time-lag effects of drought on grassland vegetation: a case study in the Chinese Loess Plateau. *J. Environ. Manag.* **261**, 110214 (2020).
32. Xu, H., Wang, X. & Zhao, C. Yang X.-m. Diverse responses of vegetation growth to meteorological drought across climate zones and land biomes in northern China from 1981 to 2014. *Agric. For. Meteorol.* **262**, 1–13 (2018).
33. Wang, Y. et al. Response of vegetation to drought in the Tibetan Plateau: Elevation differentiation and the dominant factors. *Agric. For. Meteorol.* **306**, 108468 (2021).
34. Zhang, Q., Qi, T., Singh, V. P., Chen, Y. D. & Xiao, M. Regional frequency analysis of droughts in China: A multivariate perspective. *Water Resour. Manag.* **29**(6), 1767–1787 (2015).
35. Carlson, T. N. & Ripley, D. A. On the relation between NDVI, fractional vegetation cover, and leaf area index. *Remote Sens. Environ.* **62**(3), 241–252 (1997).
36. Beck, H. E. et al. High-resolution (1 km) Köppen-Geiger maps for 1901–2099 based on constrained CMIP6 projections. *Sci. Data* **10**(1), 724 (2023).
37. Vicente-Serrano, S. et al. Performance of drought indices for ecological, agricultural, and hydrological applications. *Earth Interact.* **16**, 1–27 (2012).
38. Mann, H. B. Nonparametric tests against trend. *Econometrica* **13**(3), 245–259 (1945).
39. Yang, Z., Gong, J., Wang, S., Jin, T. & Wang, Y. Shifts bidirectional dependency between vegetation greening and soil moisture over the past four decades in China. *Sci. Total Environ.* **897** (2023).
40. Zhang, Z., Ju, W., Zhou, Y. & Li, X. Revisiting the cumulative effects of drought on global gross primary productivity based on new long-term series data (1982–2018). *Glob. Change Biol.* **28**, 3620–3635 (2022).
41. Song, Y., Wang, J., Ge, Y. & Xu, C. An optimal parameters-based geographical detector model enhances geographic characteristics of explanatory variables for spatial heterogeneity analysis: Cases with different types of spatial data. *GISci. Remote Sens.* **57** (5), 593–610 (2020).
42. Tucker, C. J., Newcomb, W. W., Los, S. O. & Prince, S. D. Mean and inter-year variation of growing-season normalized difference vegetation index for the Sahel 1981–1989. *Int. J. Remote Sens.* **12**(6), 1133–1135 (1991).
43. Fang, W. et al. Bivariate probabilistic quantification of drought impacts on terrestrial vegetation dynamics in mainland China. *J. Hydrol.* **577**, 123980 (2019).

44. Gupta, A., Rico-Medina, A. & Caño-Delgado, A. I. The physiology of plant responses to drought. *Science* **368** (6488), 266–269 (2020).
45. Zhou, Y., Wigley, B. J., Case, M. F., Coetsee, C. & Staver, A. C. Rooting depth as a key woody functional trait in savannas. *New Phytol.* **227**(5), 1350–1361 (2020).
46. Zu, K. et al. Upward shift and elevational range contractions of subtropical mountain plants in response to climate change. *Sci. Total Environ.* **783**, 146896 (2021).
47. Du, J. et al. Interacting effects of temperature and precipitation on climatic sensitivity of spring vegetation green-up in arid mountains of China. *Agric. For. Meteorol.* **269**–270 (2019).
48. Chen, T. et al. Disentangling the relative impacts of climate change and human activities on arid and semiarid grasslands in Central Asia during 1982–2015. *Sci. Total Environ.* **653**, 1311–1325 (2019).
49. Zeng, Z. et al. Legacy effects of spring phenology on vegetation growth under preseason meteorological drought in the Northern Hemisphere. *Agric. For. Meteorol.* **310**, 108630 (2021).
50. Zhan, C. et al. Drought-related cumulative and time-lag effects on vegetation dynamics across the Yellow River Basin, China. *Ecol. Ind.* **143**, 109409 (2022).
51. Liu, Z., Feng, S., Zhang, D., Han, Y. & Cao, R. Effects of precipitation, irrigation, and exploitation on groundwater geochemical evolution in the people's victory canal irrigation area, China. *Appl. Water Sci.* **13**(1), 1 (2022).
52. Bai, J., Chen, X., Yang, L. & Fang, H. Monitoring variations of inland lakes in the arid region of Central Asia. *Front. Earth Sci.* **6**(2), 147–156 (2012).
53. Chen, W. et al. Negative extreme events in gross primary productivity and their drivers in China during the past three decades. *Agric. For. Meteorol.* **275**, 47–58 (2019).
54. Jiao, K. W., Gao, J. B., Liu, Z. H., Wu, S. H. & Fletcher, T. L. Revealing climatic impacts on the temporal and spatial variation in vegetation activity across China: Sensitivity and contribution. *Adv. Clim. Change Res.* **12**(3), 409–420 (2021).

Author contributions

Conceptualization, Y.D. and H.W.; methodology, Y.D.; software, Y.D., H.Z. and H.Z.; validation, H.Z.; formal analysis, Y.D.; investigation, Y.D. and F.W.; resources, J.X. and H.W.; data curation, S.L.; writing—original draft preparation, Y.D. and S.L.; writing—review and editing, L.T., H.W. and H.Z.; visualization, F.W. and L.T.; supervision, J.X. and H.W.; funding acquisition, F.W. All authors reviewed the manuscript.

Funding

This study was supported by the National Natural Science Foundation of the People's Republic of China (U2443203,52279014), Major agricultural science and technology projects (NK202319020506), Henan Province Key Research and Development and Promotion Project (Science and Technology) (232102320257), Open Research Fund Program of State Key Laboratory of Eco-hydraulics in Northwest Arid Region, Xi'an University of Technology(Grant No.2022KFKT-3), Natural Science Foundation of Henan Province (242300421252), National Natural Science Foundation of China "Evolution of micro-topography and the response of fish habitat in sediment-laden river downstream of a reservoir" (52109085).

Declarations

Competing interests

The authors declare no competing interests.

Additional information

Correspondence and requests for materials should be addressed to F.W.

Reprints and permissions information is available at www.nature.com/reprints.

Publisher's note Springer Nature remains neutral with regard to jurisdictional claims in published maps and institutional affiliations.

Open Access This article is licensed under a Creative Commons Attribution-NonCommercial-NoDerivatives 4.0 International License, which permits any non-commercial use, sharing, distribution and reproduction in any medium or format, as long as you give appropriate credit to the original author(s) and the source, provide a link to the Creative Commons licence, and indicate if you modified the licensed material. You do not have permission under this licence to share adapted material derived from this article or parts of it. The images or other third party material in this article are included in the article's Creative Commons licence, unless indicated otherwise in a credit line to the material. If material is not included in the article's Creative Commons licence and your intended use is not permitted by statutory regulation or exceeds the permitted use, you will need to obtain permission directly from the copyright holder. To view a copy of this licence, visit <http://creativecommons.org/licenses/by-nc-nd/4.0/>.

© The Author(s) 2025